THE JOURNAL OF PHYSICAL CHEMISTRY C

Article

pubs.acs.org/JPCC

Mechanism of Oxygen Reduction in Aprotic Li–Air Batteries: The Role of Carbon Electrode Surface Structure

Alina I. Belova,[†] David G. Kwabi,[‡,⊥] Lada V. Yashina,[†] Yang Shao-Horn,[‡] and Daniil M. Itkis*[,†]

[†]Department of Chemistry, Moscow State University, Moscow, 119992, Russia

[‡]Materials Science and Engineering Department, Massachusetts Institute of Technology, Cambridge, Massachusetts 02139, United States

Supporting Information

ABSTRACT: Electrochemical oxygen reduction in aprotic media is a key process that determines the operation of advanced metal–oxygen power sources, e.g., Li–O_2 batteries. In such systems oxygen reduction on carbon-based positive electrodes proceeds through a complicated mechanism that comprises several chemical and electrochemical steps involving either dissolved or adsorbed species, and as well side reactions with carbon itself. Here, cyclic voltammetry was used to reveal the effects of imperfections in the planar sp^2 surface structure of carbon on the Li oxygen reduction reaction (Li-ORR) mechanism by means of different model carbon electrodes (highly oriented pyrolytic graphite (HOPG), glassy carbon, basal, and edge planes of pyrolytic graphite), in dimethyl sulfoxide (DMSO)-based electrolyte. We show that the first electron transfer step $O_2 + e^- \leftrightarrows O_2^-$ (followed by ion-coupling $Li^+ + O_2^- \leftrightarrows LiO_2$) does not involve oxygen chemisorption on carbon as evidenced by the independence of its rate on the carbon electrode surface morphology. The second electron transfer leading to Li_2O_2 ($Li^+ + LiO_2 + e^- \leftrightarrows Li_2O_2$) is strongly affected by the electrode surface even in highly solvating DMSO. Formation of Li_2O_2 via the electrochemical reaction could be observed only on the nearly ideal basal plane of graphite. In contrast, for more disordered electrode surfaces, (and/or bulk) the only reduction peak revealed on cyclic voltammograms corresponds to LiO_2 formation, supporting that solution-mediated mechanism for Li_2O_2 growth is more favorable in that case. We also show that increased defect concentrations on the carbon electrode surface promote the formation of Li_2CO_3 during ORR, albeit relatively slower than Li_2O_2 formation.

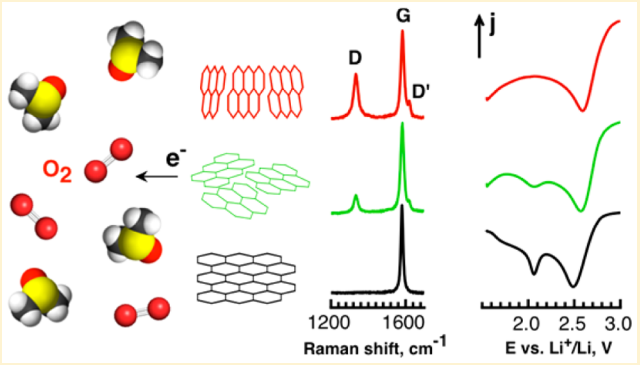

INTRODUCTION

Electrochemical oxygen reduction and evolution reactions (ORR and OER) have been of great interest for decades. This mainly arises from the advantages of using oxygen-based redox couples for energy storage and conversion. The low molecular weight and high oxidative ability of oxygen provide potentially significant improvements to the key characteristics of batteries and fuel cells, namely, working voltage and specific capacity.[1]

According to some estimates the Li–O_2 battery with aprotic electrolytes can enable specific energies up to 0.7–1 kWh/kg_{cell}.[2] Unlike fuel cell cathodes that contain ORR catalysts (mainly noble metals) providing direct 4-electron oxygen reduction to water, in Li–O_2 batteries with nonaqueous electrolytes, 2-electron reduction to main discharge product, Li_2O_2, readily occurs on plain carbon electrodes. However, despite the achievement of high capacities (up to 16 Ah/g_{carbon} for some nanostructured carbon electrodes),[3] low discharge current densities and poor cyclability limits Li–O_2 battery operation to several cycles only.[4] The reason primarily lies in slow ORR/OER kinetics and complex multistep reaction pathways. The reaction mechanism of Li-ORR on carbon electrodes has been a matter of some dispute for years, and various elementary steps that have been proposed are given in Table 1. Koutecky–Levich analysis provides an evidence that the rate-determining step of Li-ORR is one-electron reduction of oxygen.[5,6] In contrast to TBA^+-containing aprotic electrolytes, where ORR proceeds according to reaction I in Table 1, the presence of Li^+ ions results in a substantial positive shift of the ORR potential, indicating the formation of solvated lithium superoxide intermediate LiO_2 (reactions Ia, Ib).[5,7] Some authors[8,9] suggest that reaction Ib is actually composed of two time-separated steps, I and Ia, occurring in solution. Although solid-state LiO_2 can be obtained below 25 K only,[10] the existence of superoxide species on the surface of discharged electrodes was revealed by Raman spectroscopy,[11,12] X-ray diffraction (XRD),[9] X-ray absorption near edge structure (XANES),[13] and *operando* X-ray photoelectron spectroscopy

Received: December 5, 2016
Revised: December 25, 2016
Published: January 2, 2017

DOI: 10.1021/acs.jpcc.6b12221
J. Phys. Chem. C 2017, 121, 1569–1577

Table 1. Summary of Experimental Studies of Li-ORR Elementary Steps on Carbon Electrodes

N	discharge steps	electrode	electrolyte	reference
I	$O_2 + e^- \leftrightarrows O_2^-$	activated carbon	TEGDME/Li triflate	9
Ia	$O_2^- + Li^+ \leftrightarrows LiO_2$	GC	PC:DME/$LiClO_4$	8
Ib	$Li^+ + O_2 + e^- \leftrightarrows LiO_2$	activated carbon	TEGDME/Li triflate	11
		carbon black, GC	DMSO/$LiPF_6$	25
		GC	MeCN/$LiPF_6$	7
		GC	DME/LiTFSI	24
		GC	DMSO/$LiPF_6$	6
		GC	MeCN/$LiPF_6$	5
		Ketjen black	diglyme/Li triflate	26
		activated carbon	TEGDME/Li triflate	12
IIa	$LiO_2 + Li^+ + e^- \leftrightarrows Li_2O_2$	GC	DMSO/$LiPF_6$	6
		GC	DME/LiTFSI	24
IIb	$2LiO_2 \leftrightarrows Li_2O_2 + O_2$ (sol)[a]	-[c]	DMSO/LiTFSI	19
		-	TEGDME/$LiPF_6$	20
		GC	PYRTFSI/LiTFSI	27
IIc	$2LiO_2 \leftrightarrows Li_2O_2 + O_2$ (sur)[b]	activated carbon	TEGDME/$LiPF_6$	22
		activated carbon	TEGDME/$LiPF_6$	12
		activated carbon	TEGDME/$LiPF_6$	9
IIIa	$Li_2O_2 + 2Li^+ + 2e^- \leftrightarrows 2Li_2O$	carbon black, GC	DMSO/$LiPF_6$	25
		GC	DMSO/$LiPF_6$	6
IIIb	$Li_2O_2 \leftrightarrows 2Li_2O + 2O_2$	GC	DMSO/$LiPF_6$	23
IV	$LiO_2 + C \leftrightarrows Li_2CO_3$	RGO	LATP	14
		carbon black	DME/LiTFSI	24

[a]Solution-mediated reaction. [b]Surface-mediated reaction. [c]Chemical experiments.

(XPS) analysis,[14] as well as magnetic measurements.[15] The possibility of electrochemical reduction (reaction IIa) of solvated LiO_2 was suggested in a number of works[5,16] and supported by density functional theory (DFT) calculations.[17] This pathway was later proposed to become dominant at high reduction overpotentials.[18] Disproportionation of solvated LiO_2 (reaction IIb) is an alternative pathway that has been shown to occur in the electrolyte using chemical experiments where Li_2O_2 precipitates from lithium salt solutions after KO_2 addition.[19,20] This pathway prevails at low overpotentials and strongly depends on the solvent's nature.[18] Recent works report that decreasing Li^+ and O_2^- combined solvation (determined by the solvent's donor and acceptor number, respectively) lowers the stability of the LiO_2 ionic pair, thus promoting Li_2O_2 formation via disproportionation.[6,18,21] Surface-mediated disproportionation of LiO_2 species (reaction IIc) on carbon electrodes was reported as well.[9,12,22] Some evidence of Li_2O formation due to electrochemical reaction at high overpotentials (reaction IIIa)[6] or chemical processes (reaction IIIb),[23] were presented.

Besides the above-mentioned processes, carbon could also be involved in Li_2CO_3 formation due to its interaction with LiO_2.[14] CO_2 evolution during battery charge was detected by differential electrochemical mass spectrometry (DEMS) and provided evidence for the electrochemical decomposition of the Li_2CO_3 byproduct.[24]

Another important issue that affects Li-ORR mechanism is the chemical reactivity of solvents with Li_2O_2 and LiO_2 intermediate. A number of experimental studies and theoretical predictions focused on the solvent reactivity with superoxide species[28−30] and Li_2O_2[31] demonstrated that most solvents react chemically with Li−O_2 discharge products.

Although surface-mediated reactions play an important role in the Li-ORR mechanism, especially at high reduction overpotentials, much less attention is paid to the influence of electrode surface structure on Li-ORR mechanism. Carbon materials have quite complex surface chemistry due to diversity of bond types and functional groups, which can affect wetting, adsorption, electron transfer kinetics, electrocatalysis, etc.[32]

A large number of works have suggested that the basal surface of graphite is characterized by rather poor electrode kinetics, compared to edge plane, for a wide range of redox couples, including classical outer- and inner-sphere.[33] The current densities for the reduction of O_2 to O_2^- and HO_2^- are far lower on the basal plane of graphite that for O_2 reduction on pyrolytic graphite and glassy carbon in alkaline solutions.[34] This implies that O_2 reduction on carbon and graphite involves strong interaction of O_2 with functional groups on the surface.[35,36] Some evidence of the role of carbon electrode structure on discharge reactions in Li−O_2 electrochemistry was also found. DFT calculations showed that functional groups and defects in graphite sp^2 lattice affect O_2 and LiO_2 adsorption.[12,37] By evaluating the discharge performance of Li−O_2 batteries with cathodes based on oxidized carbon nanotubes with various oxygen content, the catalytic effect of oxygen functionalities in Li-ORR was examined.[38] The active edges of the graphene layers at carbon surface were reported to be indispensable for controlling the morphology of Li−O_2 deposits and improving battery performance.[39] The important role of carbon defects in carbon's reactivity toward superoxide species was also highlighted.[14]

However, experimental mechanistic studies of Li-ORR have been performed in various cell types, employing carbon materials (glassy carbon, porous activated carbon and carbon black), which possess different porosity, wettability and thus electrochemically active surface area, often using polymer binders. All this hinders correct determination of carbon surface structure effect on oxygen reduction pathways.

Here, we systematically investigate the impact of carbon defects on Li-ORR mechanisms by probing it in several model systems. We employed cyclic voltammetry on carbon disk electrodes with controllable surface structure: highly oriented pyrolityc graphite (HOPG), basal and edge plane of pyrolytic graphite (PG-basal and PG-edge, respectively), and conventional glassy carbon (GC). Dimethyl sulfoxide (DMSO), despite its reported reactivity with Li_2O_2 upon prolonged exposure,[31] was chosen as an electrolyte solvent due to its reasonable short-term stability in the presence of superoxide intermediates,[40] and higher LiO_2 disproportionation stability, which allows us to trace the disproportionation reactions on the electrode surface. Using HOPG electrode enabled separation of two electrochemical reduction peaks, which we attributed to $O_2 + e^- \leftrightarrows O_2^-$ and $LiO_2 + e^- + Li^+ \leftrightarrows Li_2O_2$. The cyclic voltammetry results show that disordered GC surface prevents further electrochemical reduction or disproportionation of LiO_2 species, in contrast to HOPG, while at the same time promoting much slower reaction with LiO_2 resulting in the

DOI: 10.1021/acs.jpcc.6b12221
J. Phys. Chem. C 2017, 121, 1569−1577

formation of lithium carbonate. LiO_2 disproportionation in solution is thus the major process that governs the Li_2O_2 formation in DMSO-based electrolyte on carbon electrodes with high amount of defects, even at high reduction overpotentials.

EXPERIMENTAL SECTION

The glassy carbon and all pyrolitic graphite disk electrodes (all 3 mm in diameter) were purchased from ALS Co., ltd. HOPG disk electrode was fabricated in-house by cutting the 3 mm diameter cylinder from the HOPG crystal parallel to its basal plane and sealing it in a polyetheretherketone (PEEK) tube with an integrated stainless steel rod providing electric contact. For XPS analysis, glassy carbon piece and HOPG crystal were used as electrodes. Glassy carbon and pyrolitic graphite electrodes were polished with 1 μm and 50 nm alumina and ultrasonicated in ethanol prior to experiments. The clean surface of HOPG electrodes was obtained by cleaving the top layer with a sticky tape.

An airtight three-electrode electrochemical cell was designed and built in-house and consisted of Ag^+/Ag reference electrode (Ag wire in a solution of 0.01 M $AgNO_3$ and 0.1 M $TBAClO_4$ in anhydrous acetonitrile (all reactants purchased from Sigma-Aldrich)) and platinum wire counter electrode. The Ag^+/Ag electrode potential was determined by calibration versus the ferrocenium/ferrocene (Fc^+/Fc) redox couple (0.02 M solution of ferrocene (98%, Sigma-Aldrich) in DMSO-based electrolyte was used). The potentials are represented versus standard Li^+/Li redox couple (−3.05 V vs SHE). Solutions of lithium perchlorate ($LiClO_4$, battery grade, Sigma-Aldrich) and/or tetrabutylammonium perchlorate ($TBAClO_4$, for electrochemical analysis, Sigma-Aldrich) in DMSO (Acros chemical company) were used as electrolytes. Water content in the electrolyte solutions was estimated to be less than 30 ppm before, and less than 100 ppm after the measurements, as determined by Karl Fischer titration. The volume of electrolyte used for each experiment was ca. 3 mL. The electrochemical cells were assembled in an Ar-filled glovebox (Labconco) where H_2O and O_2 concentrations were kept below 5 and 30 ppm, respectively.

High-purity oxygen was purged through the cell using gas inlet while gas outlet was connected to environment via hydroseal with silicone oil. The electrochemical measurements were performed with a BioLogic SAS SP-300 potentiostat/galvanostat. The electrodes were cycled continuously in potentiodynamic mode (potential sweep rate 100 mV/s) with oxygen constantly flowing until a steady cyclic voltammetric profile was obtained.

HOPG and GC electrodes after potentiostatic hold in airtight three-electrode cell were characterized by X-ray photoelectron spectroscopy (XPS) and near-edge X-ray absorption fine structure (NEXAFS) analysis. After potentiostatic hold, the electrodes were removed from the cell inside an Ar-filled glovebox (M-braun, humidity and O_2 levels lower than 0.1 ppm), washed with pure 1,2-dimethoxyethane (Sigma-Aldrich, anhydrous), and transferred to a spectrometer ultrahigh vacuum chamber without contact with air. The measurements were performed at RGBL beamline of BESSY II synchrotron (Helmholtz-Zentrum Berlin). NEXAFS spectra were recorded in total electron yield mode by measuring sample drain current. Photoemission spectra were acquired using a SPECS Phoibos 150 electron energy analyzer at a base pressure better than 5×10^{-10} mbar. Total energy resolution was not worse than 0.1 eV. The energy scale of the electron analyzer was calibrated using the Au 4f line. The reproducibility of binding energy determination was estimated to be better than 0.05 eV. Spectra were fitted by Gaussian/Lorentzian convolution functions using a Unifit 2014 data processor. Asymmetry of the sp^2 component in C 1s core-level spectra was described with Doniach−Šunjić functions. Spectral background was optimized using a combination of Shirley and Tougaard functions simultaneously with spectral fitting. Atomic fractions were calculated from peak intensities obtained at fixed kinetic energy (200 eV) normalized by theoretical photoionization cross sections[41] and photon flux.

RESULTS AND DISCUSSION

The role of carbon electrode surface structure in Li-ORR mechanisms was studied by means of cyclic voltammetry in oxygen-saturated 0.1 M $LiClO_4$ in DMSO. Carbon electrodes that were chosen for the analysis have different morphologies (Figure 1) and amount of defects according to Raman spectra

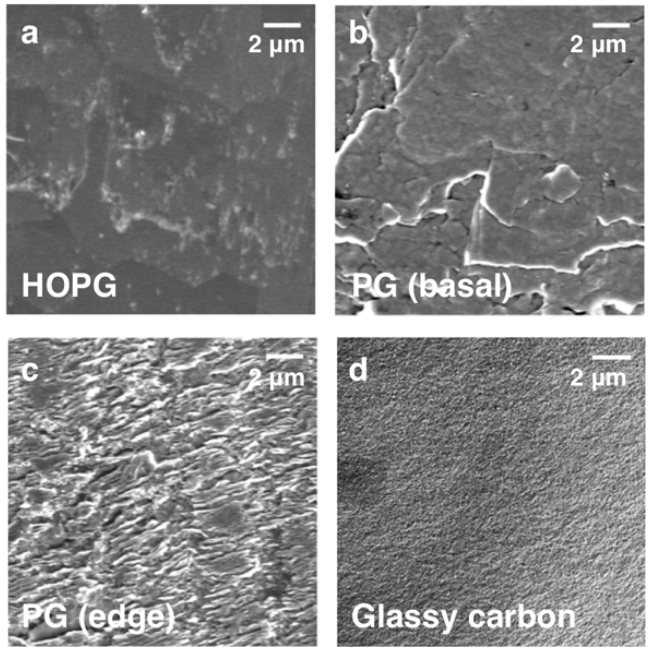

Figure 1. SEM images of the initial electrode surfaces: (a) HOPG (basal); (b) PG (basal); (c) PG (edge); (d) glassy carbon.

(Figure 2a). HOPG presents a nearly ideally ordered surface with an sp^2-hybridized carbon atom network. The PG basal surface demonstrates a disorder in lateral crystallite orientation with a certain density of domain boundaries (mean domain size is about 100 nm). Another PG electrode primarily exposes graphene layer edges to the electrolyte solution. GC electrode is a combination of the sp^2 fragments on sp^3 matrix both in bulk and at the surface.

Raman spectroscopy was used to characterize the carbon crystallinity. The Raman spectrum of HOPG electrode consists of two dominant features: G-band (1580 cm^{-1}) associated with the longitudinal optical (LO) phonon mode, and second-order dispersive 2D-band (2670 cm^{-1}). D-band feature (1370 cm^{-1}) appears in disordered carbons due to the presence of edges, stacking disorder between two layers, and atomic defects within the layer.[42] The disorder-induced D′-band (1630 cm^{-1}) is responsible for intravalley double resonance Raman process.[43] The ratio between D- and G-band integral intensities (Figure

DOI: 10.1021/acs.jpcc.6b12221
J. Phys. Chem. C 2017, 121, 1569−1577

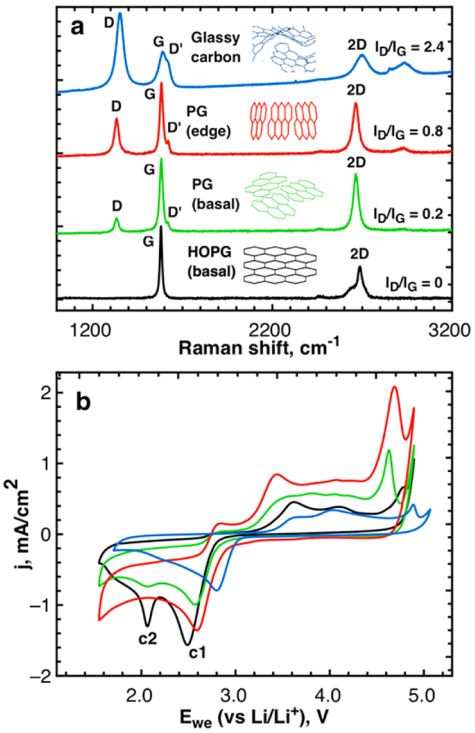

Figure 2. (a) Raman spectra of initial carbon electrodes revealing characteristic features: LO phonon mode-induced G-band and second-order dispersive 2D-band of sp^2 lattice, and disorder-induced D- and D′-bands; (b) cyclic voltammograms, recorded on different carbon working electrodes in oxygen saturated 0.1 M solution of $LiClO_4$ in DMSO. Potential sweep rate was 100 mV/s. Current densities were calculated with respect to geometric surface area of disk electrodes. Measurements were performed in a glass three-electrode cell with Pt counter electrode and Ag^+/Ag acetonitrile-based reference electrode.

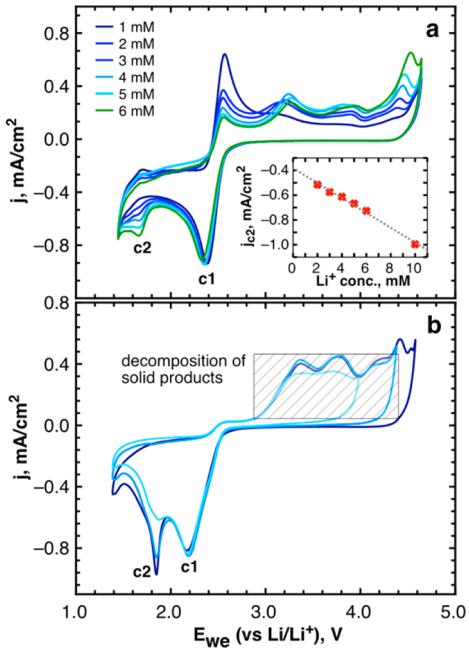

Figure 3. (a) CVs of ORR/OER at 100 mV/s in 0.1 M $TBAClO_4$ in DMSO with various concentrations of $LiClO_4$ (listed on the graph), on HOPG electrode, and c2 peak current versus Li^+ ion concentration (inset); (b) CVs of ORR/OER at 100 mV/s in 0.1 M $LiClO_4$ in DMSO on HOPG electrode with various anodic cutoff potentials.

2a) is normally used to evaluate the structural disorder of carbon materials.

Typical cyclic voltammograms of carbon electrodes at a sweep rate of 100 mV/s are shown in Figure 2b. In contrast to GC and PG-edge electrodes, HOPG and PG-basal electrodes, which have comparable surface, were found to show two well-resolved reduction peaks (c1 and c2 in Figure 2b). Peak c1 at ca. 2.5 V was always observed on glassy carbon electrodes, in either Li^+- or TBA^+-containing electrolytes and has been attributed previously to the reaction $Li^+ + O_2 + e^- \leftrightarrows LiO_2$[6,23] or $TBA^+ + O_2 + e^- \leftrightarrows TBAO_2$.[5]

Peak c2 at ca. 2 V has never been observed previously on carbon electrodes in Li^+-containing electrolytes; however, it was detected in cyclic voltammograms of Au electrodes[18] in Li^+-containing electrolytes and for glassy carbon electrodes in TBA^+-containing electrolytes.[5] It was assigned to the reactions $LiO_2 + Li^+ + e^- \leftrightarrows Li_2O_2$ or $TBAO_2 + TBA^+ + e^- \leftrightarrows TBA_2O_2$, respectively.

Similar to the previous studies that were performed on Au disk electrode,[18] c1 peak current is independent of Li^+ concentration for both HOPG and GC electrodes (Figure 3a, Figure S1). Based on that, we ascribe peak c1 to one-electron oxygen reduction to O_2^-:

$$O_2 + e^- \leftrightarrows O_2^-$$

Further ion coupling can proceed in the solution phase:

$$O_2^- + Li^+ \leftrightarrows LiO_2$$

At the same time, c2 peak current depends on Li^+ concentration (Figure 3a), and linearly scales with it in the range of 1−6 mM (Figure 3a, inset) supporting the first-order reaction with respect to Li^+-ions and indicating that LiO_2 associates were previously formed in the solution:

$$LiO_2 + Li^+ + e^- \leftrightarrows Li_2O_2$$

The reaction c2 is likely to involve LiO_2 species adsorbed on electrode surface, as it is sensitive to the electrode passivation. Successive lowering of the anodic limit while recording cyclic voltammograms increases the amount of solid product left on the surface on the following cycle, which results in substantial decrease of the c2 peak current (Figure 3b). At the same time, c1 peak current is insensitive to electrode passivation, which may indicate that reaction c1 does not involve preliminary oxygen adsorption (Figure 3b).

The anodic semicycle is very informative and reveals the decomposition of discharge products that have been generated on the electrode surface. On GC electrodes it includes several peaks that were attributed in different works to oxidation of LiO_2 (3.5 V,[44] 2.6 V[23]), Li_2O_2 (3.75 V,[44] 3.6 V,[6] 3.2 V,[23]) LiO_2^- (3.2 V[6]), Li_2CO_3 (4.5 V,[23] 4.2 V[24]) and Li_2O (4.2 V,[6] 3.8 V[23]). Previously reported galvanostatic charging experiments demonstrated that two charge plateaus on activated carbon electrodes at the potentials of 3.2 and 4 V[22] can be assigned to LiO_2 and Li_2O_2 oxidation, respectively. A small anodic peak below 2 V could be connected with the oxidation of $(TBA)_2O_2$ to $(TBA)O_2$; however, further studies are required in order to prove it.

To investigate the nature of the anodic peaks on HOPG and GC surfaces, we performed potentiostatic holding at c1 and c2 peak potentials, which was followed by linear anodic sweep voltammetry (Figure 4). After potentiostatic holding at 2.4 V (c1 peak potential for GC) and 2.0 V, the GC electrode was

DOI: 10.1021/acs.jpcc.6b12221
J. Phys. Chem. C 2017, 121, 1569−1577

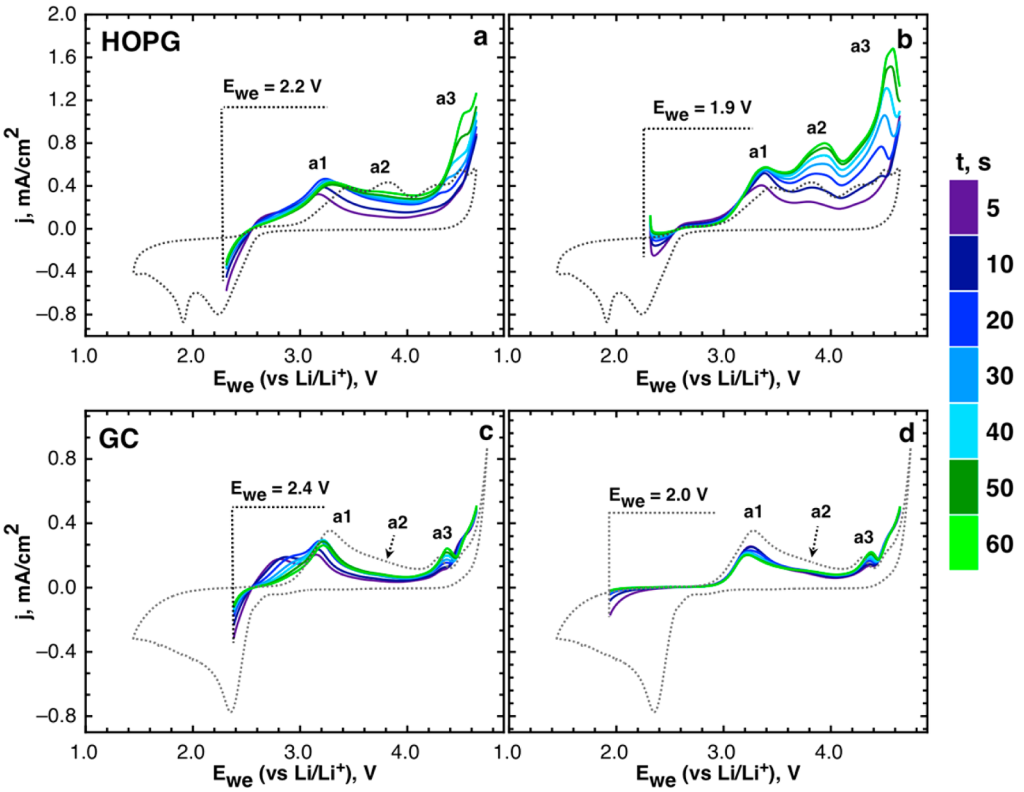

Figure 4. Anodic LSV curves at 100 mV/s in 0.1 M $LiClO_4$ in DMSO, recorded after potentiostatic holds of different duration on HOPG electrode (a, b) and on GC electrode (c, d). Hold potentials are indicated by vertical dashed lines, while durations are indicated by different colors. Thin gray dashed lines show typical cyclic voltammograms for the corresponding electrodes at the same sweep rate.

found to exhibit a single well-resolved anodic peak a1 at 3.2 V in both cases (Figure 4c,d). The HOPG electrode was held at 2.2 and 1.9 V (c1 and c2 peak potentials for HOPG, respectively), and in contrast to GC the potentiostatic hold at c2 peak potential gave rise to the additional anodic peak a2 at ca. 4 V (Figure 4a,b).

Taking into account reduction reactions that correspond to the c1 and c2 peaks according to our data and to the literature,[44] we propose the following scheme for the anodic process. We ascribe the peak a1 to adsorbed LiO_2 oxidation:

$$LiO_{2(ads)} \leftrightarrows Li^+ + O_2 + e^-$$

and peak a2 to oxidation of Li_2O_2:

$$Li_2O_{2(ads)} \leftrightarrows 2Li^+ + O_2 + 2e^-$$

The peak a2 is very weak on GC electrode, in contrast to HOPG surface, that may indicate that the surface-bound Li_2O_2 cannot be formed on defective GC electrode. On HOPG the a2 peak current increases when potentiostatic hold is carried out at lower potential (c2) enabling electrochemical LiO_2 reduction. We can assume that LiO_2 is stabilized by carbon surface defects preventing both surface-mediated disproportionation and further reduction to Li_2O_2. This result is in agreement with previous work,[22] suggesting that the structure of activated carbon electrode provides a suitable environment for surface stabilization of lithium superoxide compound. Although these species were reported to be prone to disproportionation to Li_2O_2,[22] it was shown by X-ray diffraction and Raman spectroscopy that LiO_2 can survive for several days[9] by being stabilized by carbon surface.[12] DFT calculations suggested that oxygen-containing defects on the carbon surface might be responsible for such stabilization.[37]

One more anodic peak a3, whose origin is questionable, is observed on both HOPG and GC at the potential 4.4−4.6 V (see Figure 4). This peak can be ascribed to the decomposition of byproducts generated in side-reactions with superoxide species. The anodic peak at the potentials 4.2−4.5 V was previously reported for GC electrode in dimethoxyethane (DME)-based electrolyte and was attributed to the Li_2CO_3 decomposition, as it was accompanied by CO_2 evolution according to DEMS measurements.[24] This peak also appears on anodic voltammetric sweeps after treatment of glassy carbon electrodes with KO_2 powder in Ar atmosphere.[14] In other works utilizing DMSO- and DME-based electrolytes, the anodic peak in the same region was ascribed to Li_2O[6] or LiOH decomposition,[45] as well as to the products of electrolyte side reactions.[45] Pt electrode, however, shows no peaks in the potential region >4 V in the same electrolyte solvent (see Figure S2). Taking into account that a3 peak current increases with potential holding time (Figure 4) for both GC and HOPG, it likely arises from oxidation of the species produced by reaction of carbon electrode with superoxide, e.g., Li_2CO_3.

We performed *ex situ* NEXAFS and XPS analysis of HOPG and GC electrodes recovered from Li/O_2 electrochemical cells after potentiostatic holding at c1 peak potentials in O_2-saturated 0.1 M solution of $LiClO_4$ in DMSO. The depth of discharge was equal to 0.3 $\mu Ah/cm^2$ (equivalent to the charge required to produce 16 monolayers of Li_2O_2 on electrode surface). The appearance of a Li 1s signal and increasing of O 1s intensity provides evidence of lithium- and oxygen-containing species forming on the electrode surfaces (Figure

DOI: 10.1021/acs.jpcc.6b12221
J. Phys. Chem. C 2017, 121, 1569−1577

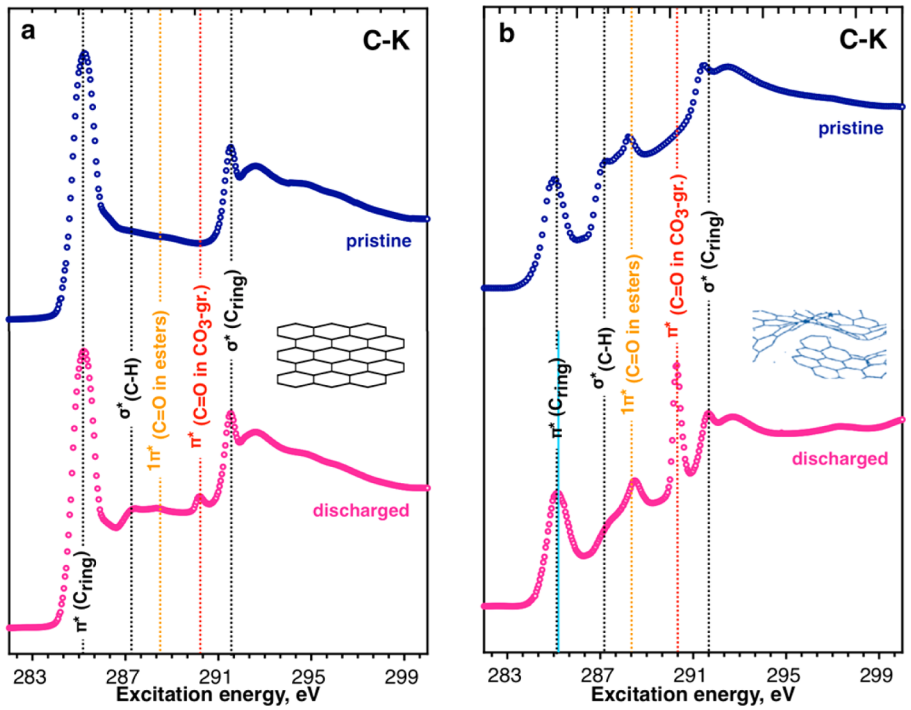

Figure 5. NEXAFS C−K edge spectra of HOPG and GC electrodes before (blue) and after (pink) potentiostatic holding at 2.2 or 2.4 V, respectively. Discharge was performed in 0.1 M $LiClO_4$ in oxygen-saturated DMSO. The cell comprised Ag^+/Ag reference electrode and Pt counter electrode. The cell was assembled and disassembled inside an Ar-filled glovebox. The HOPG and GC electrodes were transferred to the ultrahigh vacuum environment of the spectrometer under Ar atmosphere to avoid contact with ambient air.

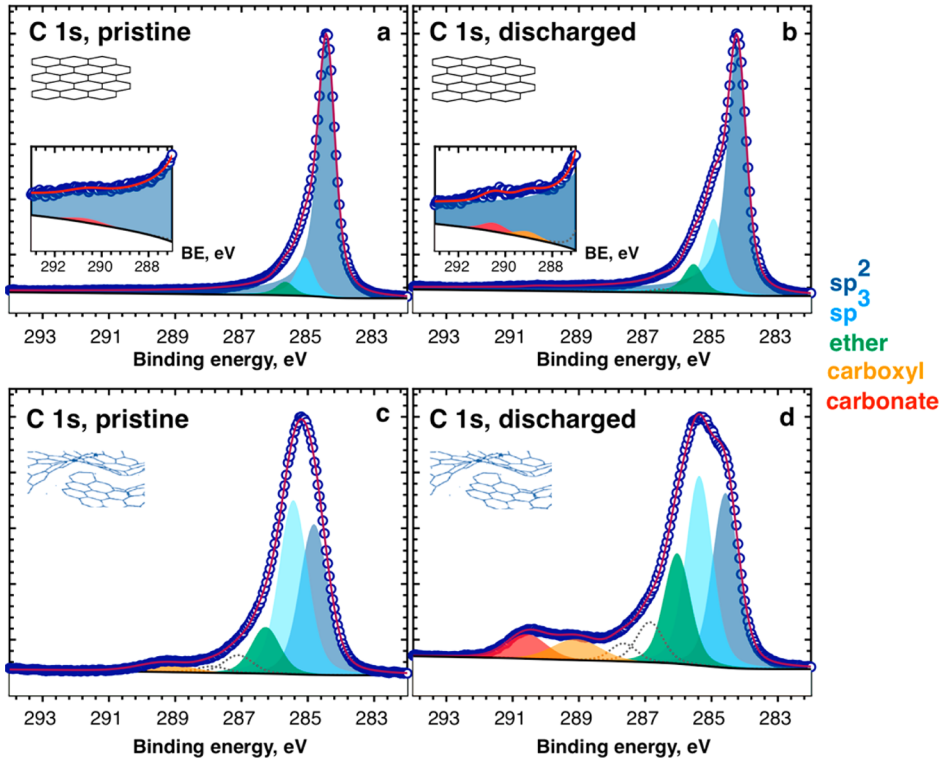

Figure 6. C 1s photoemission spectra of HOPG (a, b) and GC (c, d) electrodes before (a, c) and after (b, d) potentiostatic holding at 2.2 or 2.4 V, respectively.

S2). Special efforts were taken to ensure that no electrolyte remained on the electrode: S 2p, Cl 2p and Li 1s spectra collected before and after soaking the electrode into the electrolyte were used for monitoring proper removal of the electrolyte residues (Figure S3). Small amounts of Li- and O-containing electrolyte components were detected on the surface after soaking, which could not account for the observed increases in Li and O signals after cathodic process.

DOI: 10.1021/acs.jpcc.6b12221
J. Phys. Chem. C 2017, 121, 1569−1577

The NEXAFS C−K edge spectrum of pristine HOPG electrode (Figure 5a) demonstrates typical features for graphite lattice only: C 1s → $\pi^*(C_{ring})$ and C 1s → $\sigma^*(C_{ring})$ excitations at 285 and 291.5 eV, respectively.[46] The spectrum of pristine GC surface (Figure 6b) additionally contains features corresponding to C 1s → σ^*(C−H) excitation from aliphatic carbon atoms at 287 eV[47] and C 1s → $1\pi^*$(C═O) excitation from carboxyl groups at 288.5 eV,[47] which is expected for the highly defective structure of GC. After potentiostatic holding a sharp peak at 290.5 eV appears in spectra for both electrodes, having much higher intensity for GC. This feature was previously attributed to C 1s → π^*(C═O) excitation of carbonate groups.[47]

The quantitative estimations of relative Li_2CO_3 amount were done using XPS analysis of the same electrodes. In contrast to HOPG, Li-ORR on GC electrode lead to noticeable increase of the components located at 290.6 eV and corresponding to carbon bonded to three oxygen atoms in a carbonate group.[48]

A simultaneous growth of the component at 286 eV, often ascribed to bridging ether C−O−C groups,[49] can indicate the presence of organic or semiorganic carbonates bound to the carbon surface; however, exact determination of the type of carbonate requires additional investigation. Along with the carbonate component, a similar amount of carboxylic groups[49] appears on electrode surface after discharge (Figure 6b,d), consistent with the NEXAFS spectrum (Figure 5). The relative intensities of carbonate and carboxyl groups for both surfaces are summarized in Table 2.

Table 2. Relative Contributions of Carboxyl and Carbonate Components in XPS Spectra of HOPG and GC Electrodes[a]

electrode	I (CO_3^{2-}),%[b]	I (COO−),%[b]
HOPG (basal)	0.2	0.4
glassy carbon	5.8	2.5

[a]Spectra were measured after potentiostatic holding at c1 peak potentials of HOPG and GC (2.2 or 2.4 V, respectively). The cathodic charge passed was 0.3 μAh/cm^2 (equivalent to the charge required to produce 16 monolayers of Li_2O_2 on electrode surface). [b]Calculated with respect to the total C 1s intensity.

Both NEXAFS and XPS data (Figures 5 and 6) indicate that the amount of Li_2CO_3 and carboxylic functionalities formed during the discharge is much higher on the defective GC surface, in line with previously reported comparison of the stability of reduced graphene oxide and thermally exfoliated graphite electrodes toward superoxide species in all-solid-state cells.[14] Coupled with the hypothesis that more defective GC surface inhibits superoxide-to-peroxide conversion via disproportionation, these results allow us to assume that LiO_2 is preferably captured by the defects and then could be involved in carbonate formation, which is a relatively slow reaction, rather than transforming to peroxide product.

Although we could not determine which type of defects (vacancies or domain boundaries, layer edges, decorated or not by oxygen-containing functionalities, etc.) are responsible for carbon electrode reactivity, defective carbon surfaces evidently have sufficiently high reactivity toward superoxide species in DMSO-based electrolyte.

CONCLUSIONS

In conclusion, cyclic voltammetry technique was applied to trace the impact of carbon electrode surface structure on Li-ORR in a Li/O_2 electrochemical system in DMSO-based electrolyte. It was found that the first electron transfer step from carbon electrode to oxygen molecule does not involve oxygen chemisorption and thus does not depend on electrode structure. By contrast, further electrochemical reduction to Li_2O_2 could be observed only on the ideal basal plane of graphite and was found to be surface-mediated. Surface defects in GC stabilize LiO_2 species on the surface, preventing them from surface-mediated disproportionation and further reduction to Li_2O_2. Thus, the solution-mediated pathway should play the major role in Li_2O_2 product formation. Both NEXAFS and XPS studies of discharged HOPG and GC electrodes data indicate the formation of Li_2CO_3 as a byproduct and presumably carboxylic groups, which are more prominent on GC surface. This shows the role of carbon surface defects in carbon reactivity toward superoxide species in liquid DMSO-based electrolyte.

ASSOCIATED CONTENT

Supporting Information

The Supporting Information is available free of charge on the ACS Publications website at DOI: 10.1021/acs.jpcc.6b12221.

Cyclic voltammograms of GC, HOPG, and Pt electrodes; C 1s spectra fitting parameters; O 1s, Li 1s and S 2p, Cl 2p XPS spectra (PDF)

AUTHOR INFORMATION

Corresponding Author

*E-mail: daniil.itkis@gmail.com.

ORCID

Daniil M. Itkis: 0000-0002-6363-6669

Present Address

[⊥]Harvard John A. Paulson School of Engineering and Applied Sciences, Cambridge, Massachusetts 02137, United States.

Notes

The authors declare no competing financial interest.

ACKNOWLEDGMENTS

We thank Helmholtz-Zentrum Berlin (HZB) for the allocation of synchrotron radiation beamtimes at RGBL. Work was financially supported by Russian Science Foundation (project 16-42-01093). D.K. and Y.S.H. thank the Skolteh-MIT Center for Electrochemical Energy Storage. The work of A.I.B. at HZB was supported by the German-Russian Interdisciplinary Science Center (G-RISC).

REFERENCES

(1) Carrette, L.; Friedrich, K. A.; Stimming, U. Fuel Cells-Fundamentals and Applications. *Fuel Cells* **2001**, *1*, 5−40.

(2) Christensen, J.; Albertus, P.; Sanchez-Carrera, R. S.; Lohmann, T.; Kozinsky, B.; Liedtke, R.; Ahmed, J.; Kojic, A. A Critical Review of Li/Air Batteries. *J. Electrochem. Soc.* **2012**, *159*, R1−R30.

(3) Xiao, J.; Mei, D.; Li, X.; Xu, W.; Wang, D.; Graff, G. L.; Bennett, W. D.; Nie, Z.; Saraf, L. V.; Aksay, I. A.; et al. Hierarchically Porous Graphene as a Lithium-Air Battery Electrode. *Nano Lett.* **2011**, *11*, 5071−5078.

(4) Lu, Y.-C.; Gallant, B. M.; Kwabi, D. G.; Harding, J. R.; Mitchell, R. R.; Whittingham, M. S.; Shao-Horn, Y. Lithium−Oxygen Batteries: Bridging Mechanistic Understanding and Battery Performance. *Energy Environ. Sci.* **2013**, *6*, 750−768.

(5) Laoire, C. O.; Mukerjee, S.; Abraham, K. M.; et al. Elucidating the Mechanism of Oxygen Reduction for Lithium-Air Battery Applications. *J. Phys. Chem. C* **2009**, *113*, 20127−20134.

DOI: 10.1021/acs.jpcc.6b12221
J. Phys. Chem. C 2017, 121, 1569−1577

(6) Laoire, C. O.; Mukerjee, S.; Abraham, K. M.; Plichta, E. J.; Hendrickson, M. A. Influence of Nonaqueous Solvents on the Electrochemistry of Oxygen in the Rechargeable Lithium−Air Battery. *J. Phys. Chem. C* **2010**, *114*, 9178−9186.
(7) Abraham, K. M. Electrolyte-Directed Reactions of the Oxygen Electrode in Lithium-Air Batteries. *J. Electrochem. Soc.* **2015**, *162*, A3021−A3031.
(8) Lu, Y.-C.; Gasteiger, H. A.; Crumlin, E.; McGuire, R.; Shao-Horn, Y. Electrocatalytic Activity Studies of Select Metal Surfaces and Implications in Li-Air Batteries. *J. Electrochem. Soc.* **2010**, *157*, A1016−A1025.
(9) Zhai, D.; Lau, K. C.; Wang, H.-H.; Wen, J.; Miller, D. J.; Lu, J.; Kang, F.; Li, B.; Yang, W.; Gao, J.; et al. Interfacial Effects on Lithium Superoxide Disproportionation in Li-O_2 Batteries. *Nano Lett.* **2015**, *15*, 1041−1046.
(10) Qiu, S. L.; Lin, C. L.; Chen, J.; Strongin, M. Photoemission Studies of the Interaction of Li and Solid Molecular Oxygen. *Phys. Rev. B: Condens. Matter Mater. Phys.* **1989**, *39*, 6194−6197.
(11) Yang, J.; Zhai, D.; Wang, H.-H.; Lau, K. C.; Schlueter, J. A.; Du, P.; Myers, D. J.; Sun, Y.-K.; Curtiss, L. A.; Amine, K. Evidence for Lithium Superoxide-Like Species in the Discharge Product of a Li-O_2 Battery. *Phys. Chem. Chem. Phys.* **2013**, *15*, 3764−3771.
(12) Zhai, D.; Wang, H.-H.; Lau, K. C.; Gao, J.; Redfern, P. C.; Kang, F.; Li, B.; Indacochea, E.; Das, U.; Sun, H.-H.; et al. Raman Evidence for Late Stage Disproportionation in a Li−O_2 Battery. *J. Phys. Chem. Lett.* **2014**, *5*, 2705−2710.
(13) Gallant, B. M.; Kwabi, D. G.; Mitchell, R. R.; Zhou, J.; Thompson, C. V.; Shao-Horn, Y. Influence of Li_2O_2 Morphology on Oxygen Reduction and Evolution Kinetics in Li−O_2 Batteries. *Energy Environ. Sci.* **2013**, *6*, 2518−11.
(14) Itkis, D. M.; Semenenko, D. A.; Kataev, E. Y.; Belova, A. I.; Neudachina, V. S.; Sirotina, A. P.; Hävecker, M.; Teschner, D.; Knop-Gericke, A.; Dudin, P.; et al. Reactivity of Carbon in Lithium−Oxygen Battery Positive Electrodes. *Nano Lett.* **2013**, *13*, 4697−4701.
(15) Yang, G.; Wang, Y.; Ma, Y. A Stable, Magnetic, and Metallic Li_3O_4 Compound as a Discharge Product in a Li-Air Battery. *J. Phys. Chem. Lett.* **2014**, *5*, 2516−2521.
(16) McCloskey, B. D.; Scheffler, R.; Speidel, A.; Girishkumar, G.; Luntz, A. C. On the Mechanism of Nonaqueous Li−O_2 Electrochemistry on C and Its Kinetic Overpotentials: Some Implications for Li−Air Batteries. *J. Phys. Chem. C* **2012**, *116*, 23897−23905.
(17) Hummelshøj, J. S.; Blomqvist, J.; Datta, S.; Vegge, T.; Rossmeisl, J.; Thygesen, K. S.; Luntz, A. C.; Jacobsen, K. W.; Nørskov, J. K. Communications: Elementary Oxygen Electrode Reactions in the Aprotic Li-Air Battery. *J. Chem. Phys.* **2010**, *132*, 071101.
(18) Johnson, L.; Li, C.; Liu, Z.; Chen, Y.; Freunberger, S. A.; Ashok, P. C.; Praveen, B. B.; Dholakia, K.; Tarascon, J.-M.; Bruce, P. G. The Role of LiO_2 Solubility in O_2 Reduction in Aprotic Solvents and Its Consequences for Li-O_2 Batteries. *Nat. Chem.* **2014**, *6*, 1091−1099.
(19) Zakharchenko, T. K.; Kozmenkova, A. Y.; Itkis, D. M.; Goodilin, E. A. Lithium Peroxide Crystal Clusters as a Natural Growth Feature of Discharge Products in Li−O_2 Cells. *Beilstein J. Nanotechnol.* **2013**, *4*, 758−762.
(20) Lee, J.-H.; Yim, T.; Adams, B.; Nazar, L. F.; et al. Screening for Superoxide Reactivity in Li-O_2 Batteries: Effect on Li_2O_2/LiOH Crystallization. *J. Am. Chem. Soc.* **2012**, *134*, 2902−2905.
(21) Kwabi, D. G.; Bryantsev, V. S.; Batcho, T. P.; et al. Experimental and Computational Analysis of the Solvent-Dependent O_2/Li^+-O_2^- Redox Couple: Standard Potentials, Coupling Strength, and Implications for Lithium-Oxygen Batteries. *Angew. Chem.* **2016**, *128*, 3181−3186.
(22) Zhai, D.; Wang, H.-H.; Yang, J.; Lau, K. C.; Li, K.; Amine, K.; Curtiss, L. A. Disproportionation in Li−O_2 Batteries Based on a Large Surface Area Carbon Cathode. *J. Am. Chem. Soc.* **2013**, *135*, 15364−15372.
(23) Dilimon, V. S.; Lee, D.-G.; Yim, S.-D.; Song, H.-K. Multiple Roles of Superoxide on Oxygen Reduction Reaction in Li^+-Containing Nonaqueous Electrolyte: Contribution to the Formation of Oxide as Well as Peroxide. *J. Phys. Chem. C* **2015**, *119*, 3472−3480.
(24) McCloskey, B. D.; Speidel, A.; Scheffler, R.; Miller, D. C.; Viswanathan, V.; Hummelshøj, J. S.; Nørskov, J. K.; Luntz, A. C. Twin Problems of Interfacial Carbonate Formation in Nonaqueous Li-O_2 Batteries. *J. Phys. Chem. Lett.* **2012**, *3*, 997−1001.
(25) Trahan, M. J.; Mukerjee, S.; Plichta, E. J.; Hendrickson, M. A.; Abraham, K. M. Studies of Li-Air Cells Utilizing Dimethyl Sulfoxide-Based Electrolyte. *J. Electrochem. Soc.* **2013**, *160*, A259−A267.
(26) Xia, C.; Waletzko, M. T.; Chen, L.; Peppler, K.; Klar, P. J.; Janek, J. Evolution of Li_2O_2 Growth and Its Effect on Kinetics of Li−O_2 Batteries. *ACS Appl. Mater. Interfaces* **2014**, *6*, 12083−12092.
(27) Allen, C. J.; Hwang, J.; Kautz, R.; Mukerjee, S.; Plichta, E. J.; Hendrickson, M. A.; Abraham, K. M. Oxygen Reduction Reactions in Ionic Liquids and the Formulation of a General ORR Mechanism for Li−Air Batteries. *J. Phys. Chem. C* **2012**, *116*, 20755−20764.
(28) Bryantsev, V. S.; Giordani, V.; Walker, W.; Blanco, M.; Zecevic, S.; Sasaki, K.; Uddin, J.; Addison, D.; Chase, G. V. Predicting Solvent Stability in Aprotic Electrolyte Li-Air Batteries: Nucleophilic Substitution by the Superoxide Anion Radical ($O_2^{\bullet-}$). *J. Phys. Chem. A* **2011**, *115*, 12399−12409.
(29) Bryantsev, V. S.; Blanco, M. Computational Study of the Mechanisms of Superoxide-Induced Decomposition of Organic Carbonate-Based Electrolytes. *J. Phys. Chem. Lett.* **2011**, *2*, 379−383.
(30) Bryantsev, V. S.; Faglioni, F. Predicting Autoxidation Stability of Ether- and Amide-Based Electrolyte Solvents for Li-Air Batteries. *J. Phys. Chem. A* **2012**, *116*, 7128−7138.
(31) Kwabi, D. G.; Batcho, T. P.; Amanchukwu, C. V.; Ortiz-Vitoriano, N.; Hammond, P.; Thompson, C. V.; Shao-Horn, Y. Chemical Instability of Dimethyl Sulfoxide in Lithium−Air Batteries. *J. Phys. Chem. Lett.* **2014**, *5*, 2850−2856.
(32) McCreery, R. L. Advanced Carbon Electrode Materials for Molecular Electrochemistry. *Chem. Rev.* **2008**, *108*, 2646−2687.
(33) Kneten, K. R.; McCreery, R. L. Effects of Redox System Structure on Electron-Transfer Kinetics at Ordered Graphite and Glassy Carbon Electrodes. *Anal. Chem.* **1992**, *64*, 2518−2524.
(34) Yeager, E. Electrocatalysts for O_2 Reduction. *Electrochim. Acta* **1984**, *29*, 1527−1537.
(35) Willis, J. B.; Garten, V. A.; Weiss, D. E. A New Interpretation of the Acidic and Basic Structures in Carbons. II. the Chromene-Carbonium Ion Couple in Carbon. *Aust. J. Chem.* **1957**, *10*, 309−328.
(36) Paliteiro, C.; Hamnett, A.; Goodenough, J. B. The Electroreduction of Oxygen on Pyrolytic Graphite. *J. Electroanal. Chem. Interfacial Electrochem.* **1987**, *233*, 147−159.
(37) Xu, Y.; Shelton, W. A. Oxygen Reduction by Lithium on Model Carbon and Oxidized Carbon Structures. *J. Electrochem. Soc.* **2011**, *158*, A1177−A1184.
(38) Xia, G.; Shen, S.; Zhu, F.; Xie, J.; Hu, Y.; Zhu, K.; Zhang, J. Effect of Oxygen-Containing Functional Groups of Carbon Materials on the Performance of Li−O_2 Batteries. *Electrochem. Commun.* **2015**, *60*, 26−29.
(39) Nakanishi, S.; Mizuno, F.; Nobuhara, K.; Abe, T.; Iba, H. Influence of the Carbon Surface on Cathode Deposits in Non-Aqueous Li-O_2 Batteries. *Carbon* **2012**, *50*, 4794−4803.
(40) Takechi, K.; Higashi, S.; Mizuno, F.; Nishikoori, H.; Iba, H.; Shiga, T. Stability of Solvents Against Superoxide Radical Species for the Electrolyte of Lithium-Air Battery. *ECS Electrochem. Lett.* **2012**, *1*, A27−A29.
(41) Yeh, J. J.; Lindau, I. Atomic Subshell Photoionisation Cross Sections and Asymmetry Parameters: $1 \leq Z \leq 103$. *At. Data Nucl. Data Tables* **1985**, *32*, 1−155.
(42) Dresselhaus, M. S.; Jorio, A.; Saito, R. Characterizing Graphene, Graphite, and Carbon Nanotubes by Raman Spectroscopy. *Annu. Rev. Condens. Matter Phys.* **2010**, *1*, 89−108.
(43) Malard, L. M.; Pimenta, M. A.; Dresselhaus, G.; Dresselhaus, M. S. Raman Spectroscopy in Graphene. *Phys. Rep.* **2009**, *473*, 51−87.
(44) Peng, Z.; Freunberger, S. A.; Hardwick, L. J.; et al. Oxygen Reactions in a Non-Aqueous Li^+ Electrolyte. *Angew. Chem.* **2011**, *123*, 6475−6479.
(45) Mozhzhukhina, N.; Méndez De Leo, L. P.; Calvo, E. J. Infrared Spectroscopy Studies on Stability of Dimethyl Sulfoxide for

DOI: 10.1021/acs.jpcc.6b12221
J. Phys. Chem. C 2017, 121, 1569−1577

Application in a Li−Air Battery. *J. Phys. Chem. C* **2013**, *117*, 18375−18380.
(46) Rosenberg, R. A.; Love, P. J.; Rehn, V. Polarization-Dependent C(K) Near-Edge X-Ray-Absorption Fine Structure of Graphite. *Phys. Rev. B: Condens. Matter Mater. Phys.* **1986**, *33*, 4034−4037.
(47) Dhez, O.; Ade, H.; Urquhart, S. G. Calibrated NEXAFS Spectra of Some Common Polymers. *J. Electron Spectrosc. Relat. Phenom.* **2003**, *128*, 85−96.
(48) Dedryvère, R.; Martinez, H.; Leroy, S.; Lemordant, D.; Bonhomme, F.; Biensan, P.; Gonbeau, D. Surface Film Formation on Electrodes in a $LiCoO_2$/Graphite Cell: a Step by Step XPS Study. *J. Power Sources* **2007**, *174*, 462−468.
(49) Ganguly, A.; Sharma, S.; Papakonstantinou, P.; Hamilton, J. Probing the Thermal Deoxygenation of Graphene Oxide Using High-Resolution in Situ X-Ray-Based Spectroscopies. *J. Phys. Chem. C* **2011**, *115*, 17009−17019.

DOI: 10.1021/acs.jpcc.6b12221
J. Phys. Chem. C 2017, 121, 1569−1577